Simplify your imaging workflows

Make research imaging workflows accessible, traceable, and secure with Athena Software for Core Imaging Facilities.

Thermo Scientific™ Athena Software is a premium imaging data management platform designed for core imaging facilities that support materials science research.

Athena Software ensures traceability of images, metadata, and experimental workflows through an intuitive and collaborative web interface.

Find out more at **thermofisher.com/athena**

ThermoFisher SCIENTIFIC

ADVANCED FUNCTIONAL MATERIALS
www.afm-journal.de

A Flexible Multifunctional Triboelectric Nanogenerator Based on MXene/PVA Hydrogel

*Xiongxin Luo, Laipan Zhu, Yi-Chi Wang, Jiayu Li, Jiajia Nie, and Zhong Lin Wang**

Triboelectric nanogenerators (TENGs) represent an emerging technology in energy harvesting, medical treatment, and information technology. Flexible, portable, and self-powered electronic devices based on TENGs are much desired, whereas the complex preparation processes and high cost of traditional flexible electrodes hinder their practical applications. Here, an MXene/polyvinyl alcohol (PVA) hydrogel TENG (MH-TENG) is presented with simple fabrication, high output performance, and versatile applications. The doping of MXene nanosheets promotes the crosslinking of the PVA hydrogel and improves the stretchability of the composite hydrogel. The MXene nanosheets also form microchannels on surfaces, which not only enhances the conductivity of the hydrogel by improving the transport of ions but also generates an extra triboelectric output via a streaming vibration potential mechanism. The measured open-circuit voltage of the MH-TENG reaches up to 230 V even in a single-electrode mode. The MH-TENG can be stretched up to 200% of the original length and demonstrates a monotonical increasing relationship between the stretchable length and the short-circuit voltage. By utilizing the MH-TENG's outstanding stretchable property and ultrahigh sensitivity to mechanical stimuli, applications in wearable movement monitoring, high-precision written stroke recognition, and low-frequency mechanical energy harvesting are demonstrated.

1. Introduction

Portable, flexible, wearable, and self-powered electronic devices are highly desired to meet the new requirements in the rapid development of big data, Internet of things, and artificial intelligence.[1] However, traditional energy supply devices, such as batteries and capacitors, barely withstand a severe deformation because of their strong rigidity in structures.[2] Triboelectric nanogenerator (TENG) is a newly developing technology to realize self-powered sensing and low-frequency energy harvesting, which possesses great application potentials in flexible and wearable electronic device.[3] Flexible TENG requires that both the triboelectric and electrode layers are flexible and stretchable. Although there is a wide range of candidate materials for flexible triboelectric layer,[4] the flexible and bionic-skin electrode materials are still limited, which should perform well and stable but not be damaged by stretching, twisting, bending, and other external forces.[5] Traditional flexible conductive materials, such as conductive silver paste, silver nanowires, carbon nanotubes, and graphene, are hardly allowed to be mass-produced due to their ultrahigh cost or complicated preparation processes.[6] Therefore, it is urgent to explore and develop high-performance flexible bionic-skin electrode materials for TENGs used in electronics.

Compared with traditional metal electrodes, hydrogels are emerging flexible electrode materials attributed to their excellent stretchable, self-healing, and conductive properties.[7] However, the obvious shortcomings, such as relatively low electrical conductivity, poor mechanical and biocompatible properties, and slow response to external stimuli, have greatly restricted their practical applications.[8] In contrast, 2D transition metal carbide nanomaterial, known as MXene, possesses unique metal conductivity, hydrophilia, easy processability, high specific surface area, and excellent mechanical strength properties.[9] Therefore, an introduction of MXene into hydrogels may not only promote the conductivity of hydrogels and enhance the overall mechanical and biocompatible properties but also endow the hydrogels with new properties to realize multifunctional MXene-hydrogel materials.[10]

In this work, a flexible and stretchable TENG with mixed MXene nanosheets and polyvinyl alcohol (PVA) hydrogel

X. Luo, Dr. L. Zhu, J. Nie, Prof. Z. L. Wang
Center on Nanoenergy Research
School of Physical Science and Technology
Guangxi University
Nanning 530004, P. R. China
E-mail: zhong.wang@mse.gatech.edu

X. Luo, Dr. L. Zhu, Dr. Y.-C. Wang, J. Li, J. Nie, Prof. Z. L. Wang
CAS Center for Excellence in Nanoscience
Beijing Key Laboratory of Micro-Nano Energy and Sensor
Beijing Institute of Nanoenergy and Nanosystems
Chinese Academy of Sciences
Beijing 101400, P. R. China

Dr. L. Zhu, Dr. Y.-C. Wang, J. Li, Prof. Z. L. Wang
School of Nanoscience and Technology
University of Chinese Academy of Sciences
Beijing 100049, P. R. China

Prof. Z. L. Wang
School of Material Science and Engineering
Georgia Institute of Technology
Atlanta, GA 30332, USA

The ORCID identification number(s) for the author(s) of this article can be found under https://doi.org/10.1002/adfm.202104928.

DOI: 10.1002/adfm.202104928

encapsulated as stretchable electrodes was fabricated and named MH-TENG. A silicon rubber Ecoflex was used to act as a triboelectric layer and prevent the composite hydrogel from losing water. The MH-TENG shows an excellent output performance by a simple stretch, which can be utilized as wearable self-powered sensors for body motion monitoring. With a high sensitivity to local pinpoint stresses, the MH-TENG reveals great application potentials in handwriting recognition. A large electrical output was generated with a simple hand tapping, indicating that the MH-TENG can effectively harvest low-frequency energy derived from human movement or environmental random vibration. In general, the MH-TENGs reveal great application potentials in flexible wearable sensors, action recognition as well as power supplies.

2. Results and Discussion

The novel 2D carbide crystal $Ti_3C_2T_x$ MXene can be obtained by chemical stripping aluminum layer of ternary layered carbide Ti_3AlC_2 with hydrofluoric acid.[9b,11] The MXene belongs to $P6_3/mmc$ space group, which is a stratified and close-packed hexagonal crystal structure. In the $Ti_3C_2T_x$ MXene, Ti and C atoms are arranged alternately in the order of Ti/C/Ti/C/Ti, and T_x, representing for terminal functional groups, are distributed on the surfaces of the layered MXene, as shown in **Figure 1**a.[12] Figure 1b shows a low-magnification bright-field transmission electron microscopy (TEM) image of the layered MXene. An enlarged edge region of the TEM image illustrates a clear layered structure of MXene (Figure 1c). Selective area electron diffraction (SAED) pattern (Figure 1d) demonstrates a good single crystallinity of the MXene nanosheets, which is in good agreement with the recent report.[13] A high angle annular dark field scanning TEM (HAADF-STEM) image (Figure S1, Supporting Information) further confirms the stratified structure of the MXene nanosheets. Energy dispersive X-ray (EDX) spectroscopic mapping (Figure 1e) reveals uniform distribution of Ti, F, O, and C elements in the MXene nanosheets.

The MXene/PVA hydrogel was synthesized by a chemical crosslinking method, where the PVA solution acted as a base material.[7b,13] Sodium tetraborate and MXene powders, acting as crosslinking agents, were added into the PVA solution to form black soft solid. Optical images of pure and MXene nanosheets doped PVA hydrogel are shown in Figure S2 in the Supporting Information. MXene/PVA hydrogel could be stretched up to 1800% of the original length from 2 to 36 cm, showing better stretch properties than that of the pure PVA hydrogel (Figure S2c,d, Supporting Information). The as-fabricated MXene/PVA hydrogel possessed great self-healing ability (Figure 1f), which healed rapidly and seamlessly when the divided two parts linked together in the natural environment. The excellent self-healing and stretchable properties of the MXene/PVA hydrogel were derived from abundant surface functional groups in the MXene nanosheets, which provided additional hydrogen bond (H-bond) binding sites and hence promoted the crosslinking of the PVA hydrogel.[13,14] Figure 1g shows the schematic of the as-synthesized MXene/PVA hydrogel structure. The borate molecules were first served as the crosslinking agent to enhance the pure PVA hydrogel.[7b,15] By introducing extra H-bonds, the further doped MXene nanosheets could not only promote a primary crosslinking with the original partially free PVA molecules but also trigger a secondary crosslinking with the PVA molecular chains after crosslinking with borate. From the Fourier transform infrared (FTIR) spectra (Figure 1h), a strong H-bond peak at the wavenumber of 3000–3800 cm^{-1} was demonstrated. The Raman spectra (Figure 1i) of the MXene nanosheets and the hydrogels are basically the same as a previous report.[15] The powder X-ray diffraction (XRD) pattern of the MXene nanosheets presented prominent peaks corresponding to the (002), (006), and (008) planes while no characteristic peaks were present for the MXene/PVA hydrogel, indicating the MXene/PVA hydrogel kept in a crosslinking state (Figure 1j).[16]

Based on the excellent performance of the MXene/PVA hydrogel, we sealed the improved hydrogels with an Ecoflex silicone rubber (see Figure S3, Supporting Information). The MH-TENG was placed in the air at room temperature for 5 d and its weight only decreased from 2.98 to 2.95 g (Figure S4, Supporting Information), demonstrating the Ecoflex could effectively prevents the MXene/PVA hydrogel from losing water. After an optimized sealing process, the low velocity of losing water may be further reduced. In addition, the Ecoflex was also a high-performance triboelectric material. After the MXene/PVA hydrogel was connected with an external conductive copper wire, a flexible and stretchable single-electrode mode MH-TENG was fabricated (**Figure 2**a). Here, the MH-TENG utilizes the MXene/PVA hydrogel to serve as the electrode and also to provide ion transportation for electrostatic screening of triboelectric charges in the Ecoflex, as shown in Figure 2b. At the initial state (process (i) in Figure 2b), when a Kapton film is completely contacted with the Ecoflex of the MH-TENG under an external mechanical force, the surface charges are induced on the two materials according to the triboelectric effect, with the same amount of positive and negative triboelectric charges distributed at the Ecoflex and Kapton surfaces, respectively. Then, with the Kapton and the MH-TENG gradually separating, the positive charges on the Ecoflex are not completely shielded by the negative charges on the Kapton. The remaining positive charges on the Ecoflex will attract negative ions in the MXene/PVA hydrogel to the upper surface (process (ii) in Figure 2b). As a result, electrons from the external circuit will flow toward the hydrogel. Next, when the Kapton moves far enough, the circuit no longer generates charge movement due to the complete screening of positive charges on the Ecoflex by the negative ions in the MXene/PVA hydrogel (process (iii) in Figure 2b). Finally, when the Kapton approaching the Ecoflex, the potential difference between the two triboelectric materials decreases due to the enhanced electrostatic shielding which will repel the negative ions from the upper surface of the MXene/PVA hydrogel and urge excess electrons in the external circuit to flow into the earth (process (iv) in Figure 2b). When the Kapton contacts the Ecoflex again, the working mode returns to the state (i) and then keeps circulating.

Besides, the MXene nanosheets play another significant role in triboelectric mechanism in the MH-TENG, which is known as the streaming vibration potential (SVP) model.[17] The MXene/PVA hydrogel is a porous material that has a 3D network structure matrix containing a large amount of water.[13]

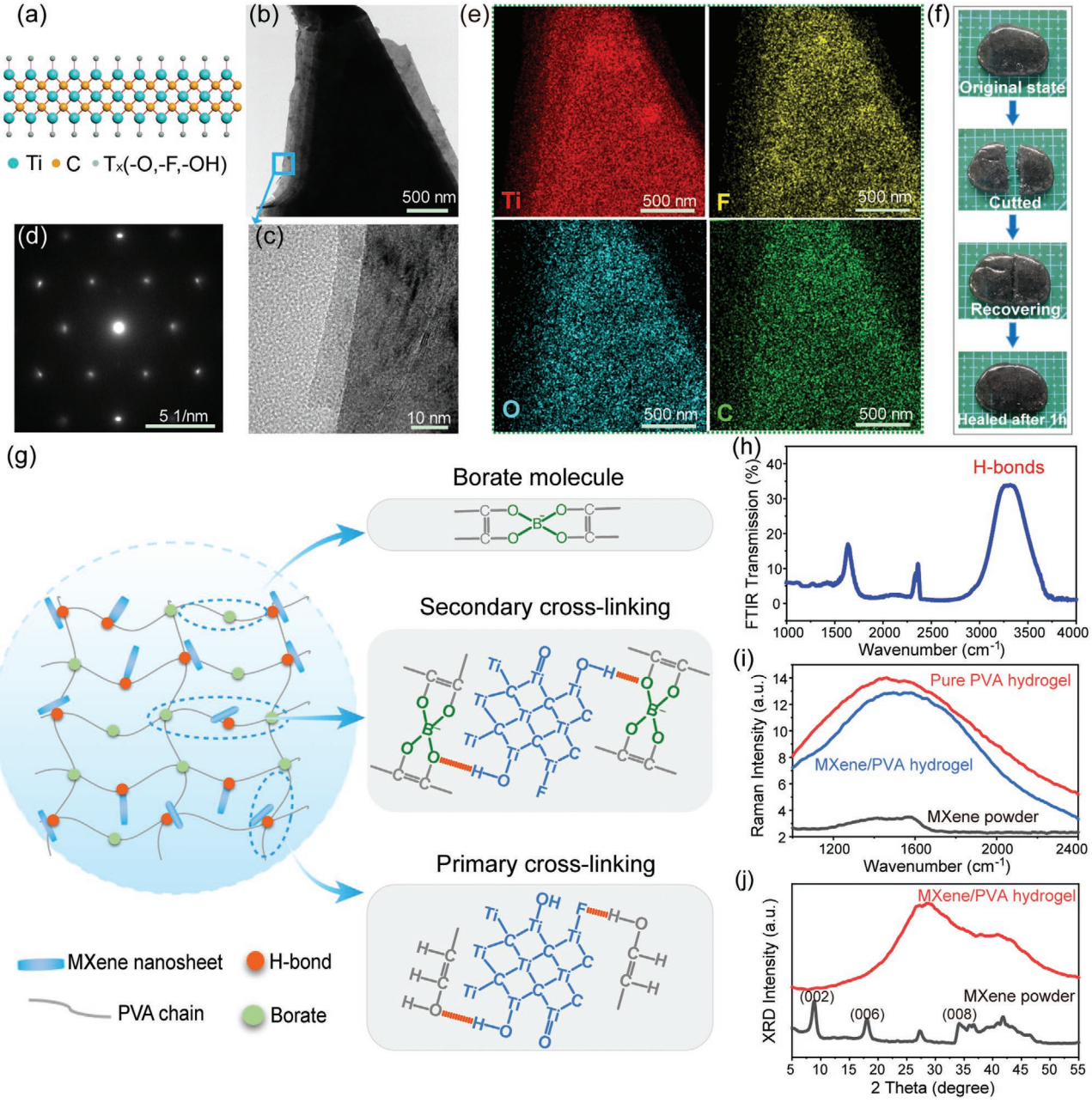

Figure 1. Microstructure and composition characterization of the MXene/PVA hydrogel. a) A schematic crystal structure of MXene. b) A low-magnification image of the MXene nanosheets acquired by TEM. c) An enlarged edge region of the MXene nanosheets from (b). d) A SAED pattern of the MXene nanosheets. e) EDX maps of the MXene nanosheets. f) Photographs of the MXene/PVA hydrogel depicting the self-healing capability. g) Schematic illustration of the as-synthesized MXene/PVA hydrogel showing the primary and secondary cross-link networks. h–j) FTIR, Raman spectra, and XRD patterns of the MXene/PVA hydrogel, respectively.

Although the MXene nanosheets can form strong H-bonds with the PVA hydrogel, the structures of the MXene nanosheets will remain unchanged (Figure 1g).[14] Therefore, the surface of MXene nanosheets can be regarded as a microchannel, which is filled with PVA molecular chains and a large amount of water. When water rubs against the MXene nanosheets, the surface of the MXene nanosheets will carry negative charges, while water near the surface of the MXene will produce positive charges, forming a double electric layer and a microchannel, which is in equilibrium without external vibration.[18] When pressure is applied on the MH-TENG, the microchannels are compressed then the water will flow out of the microchannels. The flowing water will push the positive counterbalance ions outside from the microchannels of the electric double layer but remains negative charges on the surface of the MXene. As a result, free electrons in the external circuit will be repelled into the ground and the corresponding positive charges are induced on the MXene nanosheet at the same time (process (i) in Figure 2c). When the

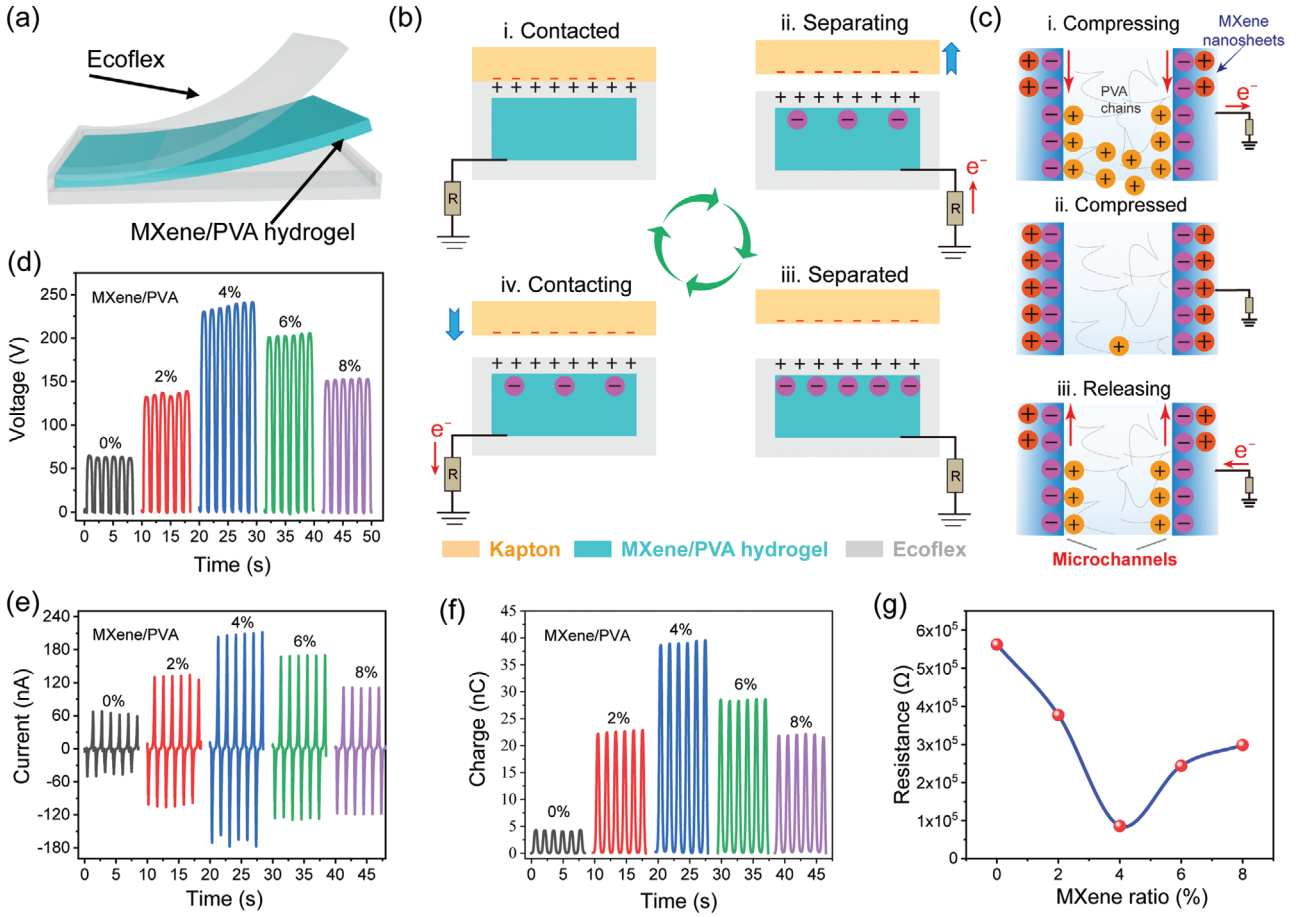

Figure 2. Operating principles and output performance of the MH-TENG. a) A schematic structure of the MH-TENG. b) A schematic working principle of the single-electrode mode MH-TENG for energy harvesting. c) The triboelectric mechanism based on microchannels of the MXene/PVA hydrogel. d) Open-circuit voltage, e) short-circuit current, and f) transferred charge amount of the MH-TENGs for different doping concentrations of MXene nanosheets. g) Resistance of the MXene/PVA hydrogel with different MXene doping concentrations.

hydrogel is compressed to the maximum, the vast majority of positive ions in the microchannels are extruded to the outside of the microchannels, and the positive and negative charges on the MXene nanosheets are in a balanced state, leading to a zero external current (process (ii) in Figure 2c). When the pressure is released, the water backflows and hence the electric double layer is formed again, resulting in a reversed external electric current (process (iii) in Figure 2c). Therefore, the MXene nanosheets can not only act as a crosslinker to improve the stretchable property of the PVA hydrogel but also help to form microchannels to promote the transport of positive ions in the MXene/PVA hydrogel after triboelectrification. More importantly, the MXene/PVA hydrogel itself can also contribute a triboelectric output under a periodic compressive force due to the SVP model, as recently reported.[17] The external electrical outputs corresponding to the contact-separating mode (Figure 2b) and the SVP mode (Figure 2c) are in the same direction, which can enhance the entire electrical output of the MH-TENG synergistically.

Based on the model of Figure 2b, we fabricated several single-electrode mode MH-TENGs with the same size, whose detailed size is shown in Figure S3 in the Supporting Information. The MXene doping concentration was studied to optimize the MH-TENG output performance (Figure 2d–f). A doping concentration of 4% in mass fraction of MXene nanosheets produced the highest output performance with the open-circuit voltage of 230 V, the short-circuit current of 270 nA, and the charge transfer amount of 38 nC when contacting with a Kapton film (with the same in-plane area as the Ecoflex) (Figure 2d–f and Figure S5 in Supporting Information), which were promoted over four times compared with those (60 V, 60 nA, and 5 nC) of the undoped PVA. The enhanced output performance manifests the significance of the MXene microchannels in the triboelectrification processes of the MH-TENG. The output performance of the MH-TENG decreases when MXene doping concentration increases from 4% to 8%. This decreased performance is probably derived from an agglomeration of excessive MXene nanosheets that greatly suppress the ion transport in hydrogel and increase the resistance of the hydrogel. The minimum resistance at 4% MXene doping concentration (Figure 2g) supports the claim.

The high flexibility and stretchability of MH-TENGs (the inset of **Figure 3**a) can generate large electrical signals by a lateral stretch due to the SVP mechanism of the microchannel

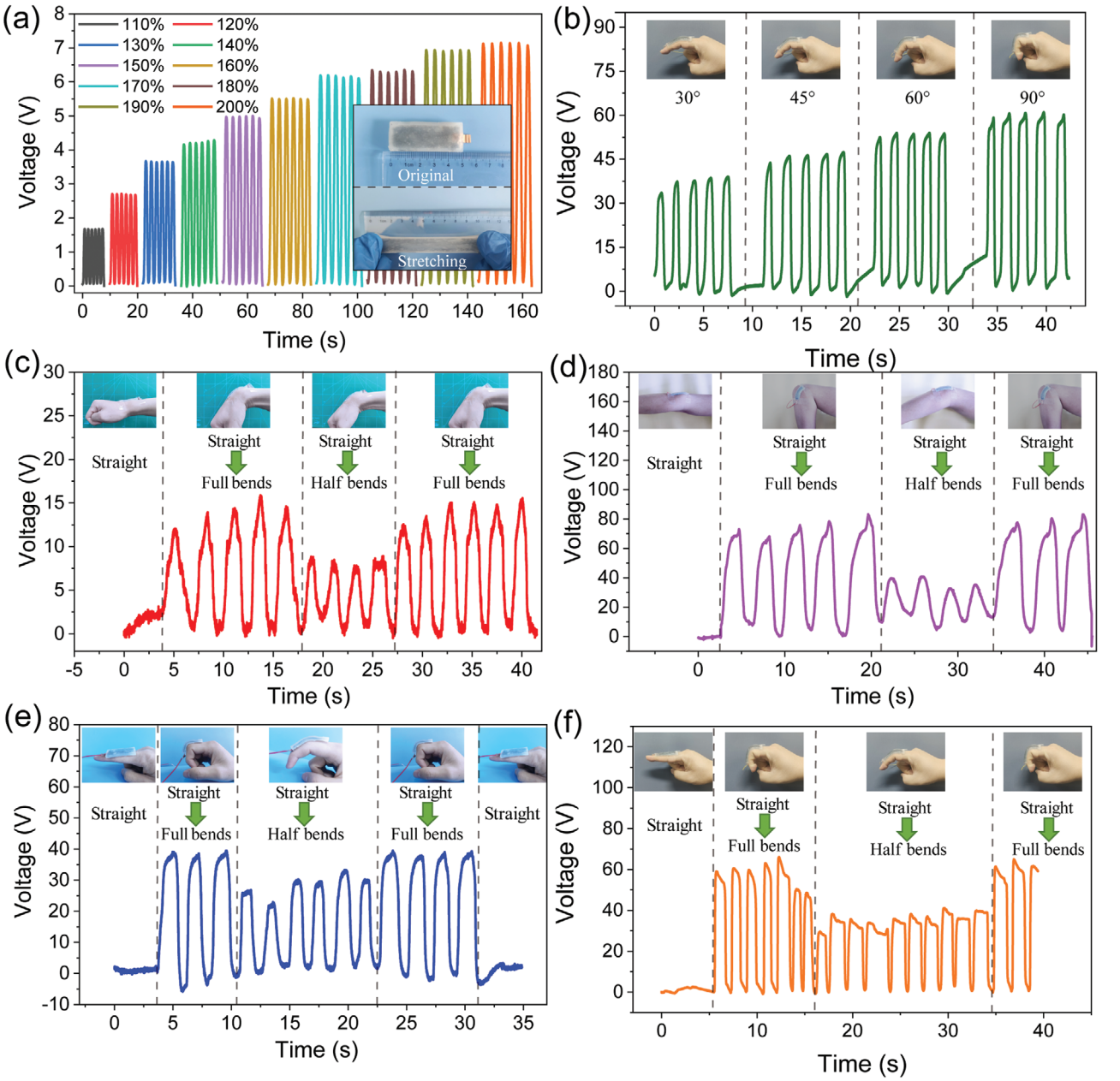

Figure 3. Output voltages generated by different stretched states and self-powered sensors for monitoring body movements. a) Output voltage as a function of stretched length, where the insets show the stretchability of the MH-TENG. b) Voltage signals of MH-TENG in response to the finger bends in 30°, 45°, 60°, and 90°. Voltage signals of the MH-TENG in response to continuous bends of c) wrist, d) elbow, and e) finger. f) Voltage signals of the MH-TENG in response to finger bends from experimenter 2.

triboelectricity. We clamped the two ends of the MH-TENG with two clamps and then fixed them on a linear motor and a 3D displacement platform, respectively (Figure S6 and Video S1, Supporting Information). Figure 3a shows the open-circuit voltage is monotonically increased with the increase of stretching length of the MH-TENG. In the SVP mechanism, the longer the stretching is, the smaller the corresponding microchannel is compressed, and the more positively charged water in the microchannel would be squeezed out of the microchannels, which will create a larger potential difference and hence attract more external charges to balance the potential difference. When the MH-TENG was stretched to 200% of the original length, it could produce an open-circuit voltage, a short-circuit current, and a transferred charge amount of 7 V, 4 nA, and 1.18 nC, respectively (Figure S7, Supporting Information). The voltage signals in Figure 3a were obtained by simple stretches of the MH-TENG, where only the SVP mechanism worked. The voltage signals in Figure 2d were generated when the MH-TENG worked at a contact-separate mode, where the voltages were derived from the synergistic effect of the triboelectrification, ions transfer, and the SVP mechanism. As a result, the voltage signals in Figure 2d are much larger than

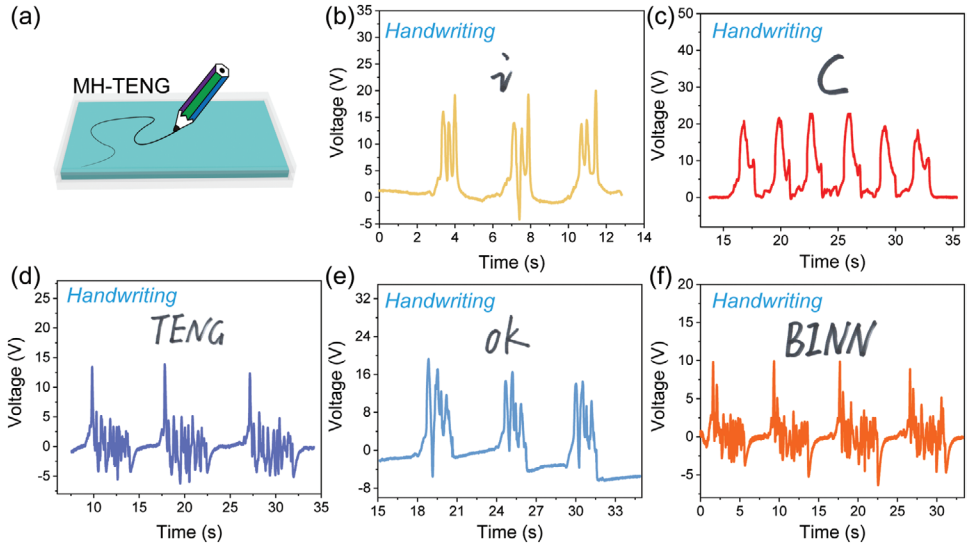

Figure 4. MH-TENG for sensing different handwritten details. a) Illustration of handwriting on the surface of MH-TENG. b–e) Repeatable voltage signals for sensing different handwriting details.

those in Figure 3a. In order to further demonstrate the importance of the SVP mechanism, we designed a set of comparative experiments. The Kapton film was used as a triboelectric material to contact and compress with the Ecoflex. The output magnitude of the contact mode is about half of that of the compression mode, as shown in Figure S8 in the Supporting Information. Two reasons account for this phenomenon. One is that the SVP mechanism is not involved in the contact mode, and the other one is that the contact area for the contact mode is smaller than that of the compression mode as the MH-TENG and Kapton films are not completely flat.

Based on the proportional relationship between the open-circuit voltage and the corresponding stretch length of the MH-TENG, the flexible and stretchable MH-TENG can be utilized as an advanced body motion monitoring sensor profited from its real-time and fast response to different movements of human body. We used tape to fix both ends of the MH-TENG to the experimenter's wrist (Figure S9a, Supporting Information), elbow (Figure S9b, Supporting Information), and finger (Figure S9c, Supporting Information), MH-TENG could translate 30°, 45°, 60°, and 90° bending angles to voltage signals (Figure 3b and Video S2, Supporting Information). And the MH-TENGs could response stably and sensitively to continuous action changes, especially to the wrist (Figure 3c and Video S3, Supporting Information) and elbow (Figure 3d and Video S4, Supporting Information) and finger (Figure 3e and Video S5, Supporting Information) half-to-full bendings. In order to prove the reliability of MH-TENG for monitoring body movement, we pasted MH-TENG on the finger of another experimenter and the same results as above can be produced (Figure 3f). What is more interesting, the voltages generated by body bendings were up to several tens volts, which were one order larger than that generated by stretching the MH-TENG to 200% of its original length, even though the actual stretched length by body bendings was not enough 200%. The two ends of MH-TENG are firmly adhered by tape, but there will be gaps between the middle part and the skin. In the process of joint bending, the skin rubs against MH-TENG and also the MH-TENG is stretched to a certain length. Therefore, this process can be regarded as the synergistic effect of the SVP model and the contact-separation model, which boosted the entire output of the MH-TENGs. Besides, the pressure applied on the microchannels during stretching only comes from an elastic force of Ecoflex, which is much smaller than those applied by an external force in Figure 2d or a compressive force due to the skin. Therefore, the MH-TENGs are good candidates for the applications of the self-powered daily and clinical body motion monitoring.

The MH-TENGs also reveal an excellent characteristic in self-powered tactile sensors. **Figure 4**a shows a schematic diagram of the MH-TENGs used for a highly sensitive handwriting recognition system, where the pen used here is a polyvinyl chloride plastic. The MH-TENGs can generate special voltage signals with different peak shapes and numbers according to the pressing force of the pen tips. The output open-circuit voltages corresponding to several representative letters ("i" (Figure 4b) and "c" (Figure 4c)) or words ("TENG" (Figure 4d), "OK" (Figure 4e), and "BINN" (Figure 4f)) wrote on the surface of the MH-TENGs by one of the authors were repeatable, where each signal group represents a complete handwritten content as shown in each inset. In order to further demonstrate the reliability of the MH-TENGs acting as self-powered sensors for handwriting recognition, the aforementioned contents were written down on the surface of the MH-TENG by another two experimenters, respectively, which are shown in Figure S10 in the Supporting Information. The output voltages of the MH-TENGs are highly repeatable when the particular author wrote down the same contents. Hence, the MH-TENGs were indicated to possess great sensitivity, reliability, and identifiability in applications of the self-powered tactile sensors. After machine learning and subsequent processing, the signal is expected to be used as a self-powered written text recognizer and an encryptor for confidential information.

Apart from the utilization in self-powered sensors, the MH-TENGs could also be used to effectively harvest mechanical

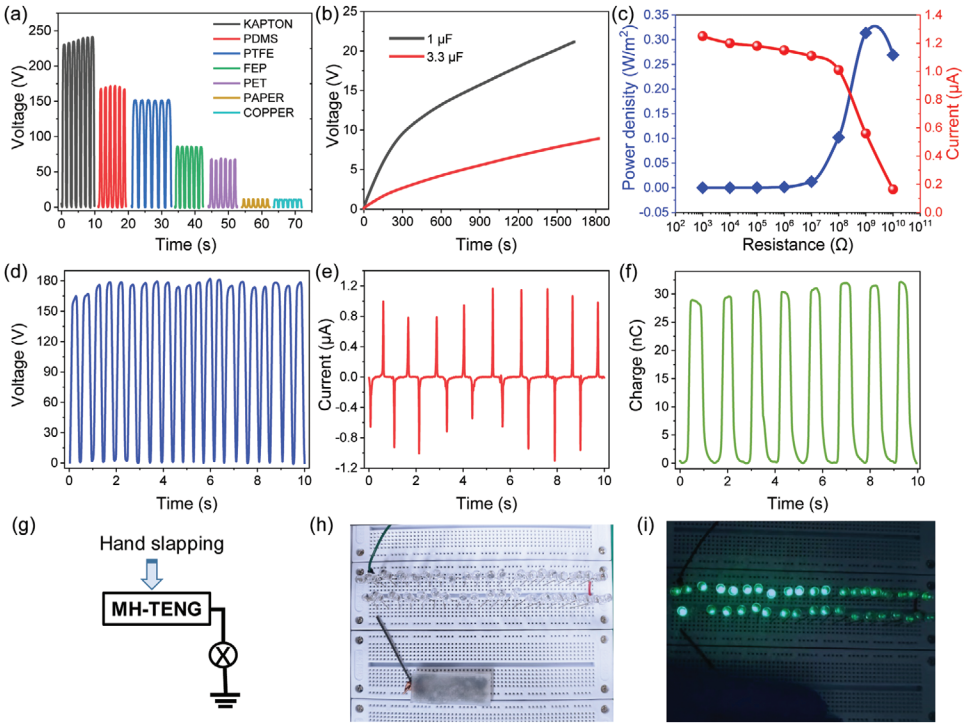

Figure 5. Demonstration of the MH-TENG for energy harvesting. a) Open-circuit voltage by replacing Kapton (see MH-TENG structure in Figure S3, Supporting Information) with other materials. b) Charging behavior of the MH-TENG with 1 and 3.3 μF capacitors under the same working frequency. c) The relationships of short-circuit current and calculated charge densities versus the resistance of the external loads. d) Open-circuit voltage, e) short-circuit current, and f) transferred charge amount of the MH-TENG with a hand slapping. g) Schematic circuit diagram of lighted LEDs by the MH-TENG. h) The original photograph of 40 LEDs connected with the MH-TENG without hand clapping. i) The photograph of 40 LEDs lighted by hand tapping of the MH-TENG.

energy in the environment. The free-standing triboelectric materials Kapton could be replaced by other abundant common materials (**Figure 5**a), showing broad applicability in different scenarios. Next, the charging capability at the same operating frequency of the MH-TENG was evaluated by charging capacitors of 1 and 3.3 μF, respectively (Figure 5b), displaying a relatively fast charging speed. From the load output characteristics in Figure 5c, the output power density, calculated by the formula $P = I2R/S$, where R and S are resistance and device area, respectively, shows an optimal output power density of 0.33 W m^{-2} with the load resistance of 10^9 Ω. Moreover, the MH-TENGs can effectively collect energy produced by human body. When the MH-TENG was treated with a hand tapping, it was able to generate an open-circuit voltage of 180 V (Figure 5d), a short-circuit current of 1.2 μA (Figure 5e), and a charge transfer amount of 32 nC (Figure 5f). Then, the MH-TENG was tried to light up several light emitting diodes (LEDs), whose circuit diagram was shown in Figure 5g. 40 LEDs were easily illumined by directly tapping the MH-TENG with hands (Figure 5h,i and Video S6, Supporting Information), revealing great application potentials of the MH-TENG in low-frequency mechanical energy harvesting.

3. Conclusion

In summary, flexible and stretchable triboelectric nanogenerators with MXene/PVA hydrogel as the electrode were fabricated. The MXene nanosheets were found to not only promote the crosslinking of the PVA hydrogel but also form microchannels inside the hydrogel, which promoted the stretchability of the composite hydrogel, enhanced the ion transport, and also induced an extra output via the SVP mechanism of microchannel triboelectricity. An optimal doping concentration of MXene nanosheets for the MH-TENGs was demonstrated to be 4%. The MH-TENG possesses outstanding stretchable property and ultrahigh sensitivity to mechanical stimuli, revealing great application potentials in wearable self-powered body movement monitoring and high-precision written stroke recognition. Besides, the free-standing triboelectric materials for the MH-TENGs can be combined with various materials to show huge potentials in low-frequency mechanical energy harvesting. It is worth noting that the MH-TENG is degradable and environmentally friendly, which is suitable with the environmental protection concept advocated at present.

4. Experimental Section

Materials: Poly(vinyl alcohol) 1788 ([—CH_2CHOH—]$_n$, alcoholysis degree 87.0–89.0% (mol mol^{-1}), molecule weight: 44.05) was supplied by Shanghai Aladding Biochemical Technology Co., Ltd. Sodium tetraborate ($Na_2B_4O_7$ anhydrous, ≥99%, molecule weight: 201.22) was purchased from Shanghai Macklin Biochemical Co., Ltd. $Ti_2C_3T_x$ (MXene) multilayer nanosheets (thickness 100–200 nm, purity 54–68 wt%) were purchased

from Jiangsu XFNANO materials Tech Co., Ltd. Ecoflex 00-50 silicone rubber (Total Net Wt. 0.90 kg) was purchased from Smooth-On company, USA.

Synthesis of MXene/PVA Hydrogel: MXene/PVA hydrogel was synthesized by a chemical-crosslinking method. First, PVA solution(8 wt%) was obtained by PVA 1788 white powder (0.4 g) dissolved in deionized water (DI water, 5 mL) with magnetic stirring at 90 °C for 5 h until all the powders have dissolved. At the same time, sodium tetraborate solutions with a concentration of 4 wt% were prepared by dissolving sodium tetraborate in DI water at 50 °C and kept shaking the solutions until the particles were completely dissolved. After the prepared sodium tetraborate solutions were cooled to room temperature, the MXene nanosheets of different weight ratio were mixed into the solutions and followed by an ultrasonic treatment of 1 h in order to make the MXene nanosheets evenly dispersed in the solutions. Finally, the PVA solutions and the crosslinking agent were slowly mixed to obtain the MXene/PVA hydrogel.

Fabrication of the MH-TENGs: The MH-TENG was a sandwiched structure with Ecoflex as top and bottom layers and hydrogel layer encapsulated inside the Ecoflex, whose detailed structure and size were depicted in Figure S3 in the Supporting Information. Ecoflex 00-50 silicone rubber (1 g, purchased from Smooth-On Company, USA) was transferred to a prefabricated 2×5 cm^2 rectangular model, pumped with vacuum to remove air bubbles, and then kept it at room temperature for 3 h to fabricate the bottom layer. Next, the prepared fix-sized MXene/PVA hydrogel was put on the center of the Ecoflex silicone rubber and attached a conductive copper foil as an external electrode. Then, the upper Ecoflex with the same quality as the bottom one was poured into the model and then performed the same vacuum, solidify processes as the bottom layer. Since the hydrogel was not completely covered, the upper and bottom layers were connected together which could effectively prevent the MXene/PVA hydrogel from losing water.

Characterization of Materials and the MH-TENGs: A Thermo Fisher Scientific Themsis-Z S/TEM was used for the TEM, HAADF-STEM, and EDX data acquisition. The microscope was operated at 300 kV, equipped with a field emission electron gun high brightness source, an image aberration corrector, a probe aberration corrector, and a Super-X EDX detector system consisting of four silicon drift detectors. The FTIR spectra were obtained by a spectrometer (Bruker, Vertex80V). Raman spectra were recorded with a laser confocal Raman spectrometer (LabRAM HR Evolution). The XRD patterns were measured with a powder XRD (Bruker, D8 ADVANCE). Electrical resistivity measurements for different concentrations MXene/PVA hydrogel and pure PVA hydrogel samples were acquired by a Keithley 4200-SCS Semiconductor Characterization System and the resistance value was calculated as the ratio of average voltage divided by average current. A step motor (LinMoE1100) was used to provide the input of mechanical motions for research of the triboelectric mechanisms. The open-circuit voltage, short-circuit current, and transferred charge amount were recorded by a Keithley 6514 electrometer. Signed informed consent was obtained from all the volunteers who participated in the experiments.

Supporting Information

Supporting Information is available from the Wiley Online Library or from the author.

Acknowledgements

X.L. and L.Z. contributed equally to this work. This research was supported by the National Natural Science Foundation of China (Grant Nos. 11704032 and 51432005), the National Key R&D Project from Minister of Science and Technology (2016YFA0202704), and the Beijing Municipal Science and Technology Commission (Z171100000317001, Z171100002017017, and Y3993113DF).

Conflict of Interest

The authors declare no conflict of interest.

Data Availability Statement

Research data are not shared.

Keywords

flexible and wearable, hydrogels, MXenes, self-powered sensors, triboelectric nanogenerators

Received: May 24, 2021
Revised: June 24, 2021
Published online:

[1] a) S. Chu, A. Majumdar, *Nature* **2012**, *488*, 294; b) Y. Song, N. Wang, C. Hu, Z. L. Wang, Y. Yang, *Nano Energy* **2021**, *84*, 105919; c) Z. L. Wang, *Nano Energy* **2019**, *58*, 669.
[2] W. Fu, K. Turcheniuk, O. Naumov, R. Mysyk, F. Wang, M. Liu, D. Kim, X. Ren, A. Magasinski, M. Yu, X. Feng, Z. L. Wang, G. Yushin, *Mater. Today* **2021**, https://doi.org/10.1016/j.mattod.2021.01.0261369.
[3] a) X. Pu, M. Liu, X. Chen, J. Sun, C. Du, Y. Zhang, J. Zhai, W. Hu, Z. L. Wang, *Sci. Adv.* **2017**, *3*, e1700015; b) R. Cheng, K. Dong, P. Chen, C. Ning, X. Peng, Y. Zhang, D. Liu, Z. L. Wang, *Energy Environ. Sci.* **2021**, *14*, 2460; c) Y. Yang, N. Sun, Z. Wen, P. Cheng, H. Zheng, H. Shao, Y. Xia, C. Chen, H. Lan, X. Xie, C. Zhou, J. Zhong, X. Sun, S. Lee, *ACS Nano* **2018**, *12*, 2027; d) Y. Peng, M. Que, H. E. Lee, R. Bao, X. Wang, J. Lu, Z. Yuan, X. Lia, J. Tao, J. Sun, J. Zhai, K. J. Lee, C. Pan, *Nano Energy* **2019**, *58*, 633.
[4] H. L. Wang, Z. H. Guo, G. Zhu, X. Pu, Z. L. Wang, *ACS Nano* **2021**, *15*, 7513.
[5] C. Ning, K. Dong, R. Cheng, J. Yi, C. Ye, X. Peng, F. Sheng, Y. Jiang, Z. L. Wang, *Adv. Funct. Mater.* **2020**, *31*, 2006679.
[6] a) H. M. Chen, Y. Xu, J. S. Zhang, W. T. Wu, G. F. Song, *Nano Energy* **2019**, *58*, 304; b) X. X. Chen, Y. Song, H. T. Chen, J. X. Zhang, H. X. Zhang, *J. Mater. Chem. A* **2017**, *5*, 12361; c) G. H. Lim, S. S. Kwak, N. Kwon, T. Kim, H. Kim, S. M. Kim, S. W. Kim, B. Lim, *Nano Energy* **2017**, *42*, 300.
[7] a) D. Bao, Z. Wen, J. Shi, L. Xie, H. Jiang, J. Jiang, Y. Yang, W. Liao, X. Sun, *J. Mater. Chem. A* **2020**, *8*, 13787; b) X. Jing, H. Li, H. Y. Mi, P. Y. Feng, X. Tao, Y. Liu, C. Liu, C. Shen, *ACS Appl. Mater. Interfaces* **2020**, *12*, 23474; c) W. Xu, L. B. Huang, M. C. Wong, L. Chen, G. X. Bai, J. H. Hao, *Adv. Energy Mater.* **2017**, *7*, 1601529.
[8] S. Hong, D. Sycks, H. F. Chan, S. Lin, G. P. Lopez, F. Guilak, K. W. Leong, X. Zhao, *Adv. Mater.* **2015**, *27*, 4035.
[9] a) W. T. Cao, H. Ouyang, W. Xin, S. Y. Chao, C. Ma, Z. Li, F. Chen, M. G. Ma, *Adv. Funct. Mater.* **2020**, *30*, 2004181; b) M. Naguib, V. N. Mochalin, M. W. Barsoum, Y. Gogotsi, *Adv. Mater.* **2014**, *26*, 992; c) A. Rodriguez, M. S. Jaman, O. Acikgoz, B. Wang, J. Yu, P. G. Grutzmacher, A. Rosenkranz, M. Z. Baykara, *Appl. Surf. Sci.* **2021**, *535*, 147664; d) L. J. Yin, Y. T. Li, X. C. Yao, Y. Z. Wang, L. Jia, Q. M. Liu, J. S. Li, Y. L. Li, D. Y. He, *Nano-Micro Lett.* **2021**, *13*, 57. e) D. Tan, C. Jiang, X. Cao, N. Sun, Q. Li, S. Bi, J. Song, *RSC Adv.* **2021**, *11*, 19169; f) N. A. Shepelin, P. C. Sherrell, E. N. Skountzos, E. Goudeli, J. Zhang, V. C. Lussini, B. Imtiaz, K. A. S. Usman, G. W. Dicinoski, J. G. Shapter, J. M. Razal, A. V. Ellis, *Nat. Commun.* **2021**, *12*, 3171.
[10] Y. Z. Zhang, J. K. El-Demellawi, Q. Jiang, G. Ge, H. Liang, K. Lee, X. Dong, H. N. Alshareef, *Chem. Soc. Rev.* **2020**, *49*, 7229.

[11] M. Naguib, M. Kurtoglu, V. Presser, J. Lu, J. Niu, M. Heon, L. Hultman, Y. Gogotsi, M. W. Barsoum, *Adv. Mater.* **2011**, *23*, 4248.
[12] M. Malaki, R. S. Varma, *Adv. Mater.* **2020**, *32*, 2003154.
[13] Y. Z. Zhang, K. H. Lee, D. H. Anjum, R. Sougrat, Q. Jiang, H. Kim, H. N. Alshareef, *Sci. Adv.* **2018**, *4*, eaat0098.
[14] Y. Cai, J. Shen, C. W. Yang, Y. Wan, H. L. Tang, A. A. Aljarb, C. Chen, J. H. Fu, X. Wei, K. W. Huang, Y. Han, S. J. Jonas, X. Dong, V. Tung, *Sci. Adv.* **2020**, *6*, eabb5367.
[15] M. Salauddin, S. M. S. Rana, M. Sharifuzzaman, M. T. Rahman, C. Park, H. Cho, P. Maharjan, T. Bhatta, J. Y. Park, *Adv. Energy Mater.* **2020**, *11*, 2002832.
[16] R. Ricciardi, F. Auriemma, C. De Rosa, F. Laupretre, *Macromolecules* **2004**, *37*, 1921.
[17] K. H. Lee, Y. Z. Zhang, Q. Jiang, H. Kim, A. A. Alkenawi, H. N. Alshareef, *ACS Nano* **2020**, *14*, 3199.
[18] H. Zhang, J. Yu, X. Yang, G. Gao, S. Qin, J. Sun, M. Ding, C. Jia, Q. Sun, Z. L. Wang, *ACS Nano* **2020**, *14*, 3461.